Light Sheet Generation for a Multi-Region Optical Trap for Ultracold Atomic Gases

Light Sheet Generation for a Multi-Region Optical Trap for Ultracold Atomic Gases

Daniel Huffman

February 2024

Abstract

By cooling down lithium-6 atoms to nano-Kelvin temperatures and tuning the magnetic field to Feshbach resonance, we can effectively create a strongly correlated quantum degenerate Fermi gas system that is then trapped in our multi-region optical trap. As the atoms are loaded into the trap, we separate the spin states and shine light sheets to divide the different regions so we can study the thermodynamic and spin transport evolution once the light sheet is removed. We showcase the design of the optical set up that images four light sheets onto the atoms to create three regions within the trap. We also describe the functionality of the digital micromirror device (DMD) that is used to shape the intensity profile of the light sheets created. Additionally, we present a method for improving the efficiency of the DMD by preshaping the light. Finally, we introduce our work on half-toning the light sheets in an effort to create a uniform intensity distribution of the light sheets by turning certain mirrors off on the DMD in an algorithmic fashion.

1 Introduction

Studying ultra-cold atoms allows us to investigate the properties of many-body systems in controllable conditions as opposed to condensed matter experiments that are bound by the material used. By choosing a quantum degenerate Fermi gas, we can tune magnetic fields to the Feshbach resonance and run quantum simulations to study the gas in the strongly interacting regime, particularly with nonequilibrium systems. Understanding these systems will give better insight into such as superconductivity in materials and the cores of white dwarf and neutron stars. In addition, these quantum simulations can be used to further explore the Hubbard model in low temperature settings. For our experiments, we will be utilizing a lithium-6 atomic gas since it is a fermion that has well studied transition properties making it an ideal candidate for laser cooling. After the multiple stages of cooling, the Li-6 gas is trapped in a ring beam and separated by spin-state via an applied magnetic field. Once sufficiently split, we would then shine light sheets into the trap creating three regions of atoms in spin polarized or mixed spin states. The light sheets are produced by pre-shaping the four laser beams with a cylindrical lens before shining them onto the DMD to shape the profile of the intensity produced. With this set up, we would be equipped to conduct three major experiments: Joule expansion (where we trap all the atoms on one side and ramp down the barrier separating the two sides), transport at the normal-superfluid (NS) interface (which ramps down the barrier between the mixed region and one of the other regions), and the transport through the bulk (which ramps down both barriers of the mixed region) to study spin-transport.

2 Background

2.1 Quantum Degenerate Fermi Gas

As the name might suggest, a Fermi gas is a gas made up of fermions. A quantum degenerate Fermi gas is a special type of Fermi gas where the temperature, T, is lower than the Fermi temperature, T_F. This means that approximately every particle in the gas is in the lowest possible energy state, and since they are all fermions they should necessarily not all be in the ground state because of the Pauli exclusion principle. These gases are a very popular choice for atomic experiments because not only

is it easily controllable since we can tune their interaction strengths, but these gases can be used to run experiments to simulate conditions that are otherwise inaccessible to us. For example, since the inward pressure of gravity compresses the atoms into their lowest energy state possible (thus satisfying $T < T_F$), the cores of neutron stars are considered degenerate matter and we can therefore study how transport in these materials work in the lab. By tuning the magnetic fields to the Feshbach resonance, we make the gas strongly interacting facilitating the creation of Cooper pairs leading to superfluidity.

2.2 Dipole Potential

Optical traps for atoms, much like our multi-region trap, rests on the properties of dipole potentials and the forces they can induce. When neutral atoms are subject to an outside electric field, like a laser light source, the different charges in the atom become polarized creating a dipole in the field. This dipole is then able to interact with the driving field with a potential profile given by $U_{dip} = -\frac{1}{2}\langle \mathbf{p} \cdot \mathbf{E} \rangle$ where $\mathbf{p}$ is the dipole moment, $\mathbf{E}$ is the driving field, and the angle brackets represent the time average of the product of the two. Since we are dealing with streams of photons hitting these atoms, in general there will also be another main effect of scattering the radiation power due to the absorption and emission of the incoming photons by the atom quantified by the scattering rate $\Gamma_{sc}(\mathbf{r})$. However, for the purposes of an optical trap, we want the scattering to be at a minimum since we only want the induced force of the field and we can achieve this by being in the far-detuned regime (which means that the laser light detuning $\Delta \equiv \omega - \omega_0$ is much greater than the atomic linewidth Γ, $\Delta \ll \Gamma$). With these constraints, we can write the potential profile in terms of the atomic resonance frequency ω_0, the frequency ω and intensity $I(\mathbf{r})$ of the light, as well as the spontaneous decay rate of the excited state atoms Γ to give us

$$U_{\text{dip}}(\mathbf{r}) = -\frac{3\pi c^2}{2\omega_0^3}\left(\frac{\Gamma}{\omega_0 - \omega} + \frac{\Gamma}{\omega_0 + \omega}\right) I(\mathbf{r}). \tag{1}$$

While this equation does work, many experiments tune the laser close enough to the resonance frequency such that $\Delta \ll \omega_0$ which lets us simplify this equation using the well-known *rotating wave approximation* (RWA) (Look at Grimm and talk to Sommer). This allows us to ignore the terms with a large frequency, namely the $\frac{\Gamma}{\omega_0+\omega}$ term. The dipole potential is now given by

$$U_{\text{dip}}(\mathbf{r}) = \frac{3\pi c^2}{2\omega_0^3}\frac{\Gamma}{\Delta} I(\mathbf{r}) \tag{2}$$

Qualitatively, we can immediately recognize two types of detuning that will result in different forces from equations 1 and 2: *red detuning* ($\Delta < 0$) and *blue detuning* ($\Delta > 0$). When the light is red detuned, the dipole potential becomes negative, creating an attractive force between the atoms and the light. Similarly, in the blue detuned case the potential remains positive creating a repulsive force that the atoms feel from the light[4]. In our set up, we will be utilizing both regimes and cases of detuning to trap the atoms. Compared to the atoms ($\lambda_{\text{Li-6}} = 671nm$), the infrared beam of the ODT ($\lambda_{\text{ODT}} = 1064nm$) has a much lower frequency making it a far, red detuned light source that exerts an attractive force (using Eq.1) in all directions perpendicular to the axis of propogation, holding the atoms in the center of the beam. By contrast, the light sheets and ring beam ($\lambda_{\text{LS}} = \lambda_{\text{Ring}} = 638nm$) will be blue detuned to provide a repulsive force (using Eq.2) on the atoms and keep them away from the barriers.

2.3 Cooling Process

In order to get the atoms cold enough to perform our experiments, they must be put through multiple stages of cooling. The first stage is the Zeeman slower which is a long tube that utilizes laser cooling which is a process where we can shine resonant frequency light in the opposite direction of the atoms to slow them down. This happens because as the atoms move through the tube, they absorb a photon and emit it in a random direction. Because of the Doppler shift, only the atoms moving against the laser will see a resonant light frequency, meaning the net momentum kick will ultimately be in the direction the laser is propagating, slowing the gas down. Once the gas has been sufficiently cooled to its new temperature, it's new speed now prevents anymore of the gas from absorbing the laser light since the Doppler shift has changed. To fix this, we can exploit the Zeeman effect and apply

a magnetic field to shift the energy levels of the atoms so that they again respond to the laser light and get cooled more. By decreasing the magnetic field applied as the atoms move down the chamber, we can effectively cool the atoms multiple times until they are ready for the next stage. At this point, we can load the atoms into the magneto-optical trap (MOT) which consists of two coils with opposite currents as well as six counter-propagating laser beams (two for each Cartesian coordinate axis). The two coils produce a gradient magnetic field that cascades down to the center of the trap where it equals zero.

Once cold enough, we can increase the magnetic field gradient for further cooling before it moves to D1 or Gray molasses cooling. When this is done, the last trap we use is the (crossed) optical dipole trap (ODT) where we simply shine an infrared laser on the cloud. With a wavelength of $\lambda_{IR} = 1064nm$, this will behave similarly to the ring beam potential described in the previous section meaning that the laser is creating an attractive harmonic potential whose depth is proportional to its intensity. By crossing the ODT, we can increase the intensty of the trap and hold more atoms for longer. Once here, we can apply our last stage of cooling before loading into the multi-region trap which is the evaporative cooling. Evaporative cooling works by slowly decreasing the intensity of the laser light so that the potential well becomes shallower and letting the atoms that are hot enough jump out. After a while, the total cloud will rethermalize to a temperature lower than what it began with since all the high energy particles were lost. Ideally, this allows us to reach the nanoKelvin regime in our gas that will then be loaded into the multi-region trap and experimented with[1].

3 Experiments

3.1 Multi-Region Trap

Once the atoms are cooled enough from the ODT to start experimentation, the atoms are loaded into a multi-region box trap pictured in Fig.1 which is where most of our ultracold atom experiments will take place. They are initially trapped with a ring beam with a diameter of $40\mu m$. They are then subject to a magnetic field that will separate the atoms by spin so that the outer regions are spin polarized while the middle region is a mix of spins. The $3 - 4\mu m$ light sheets we generate will then be imaged onto the trap splitting it into three regions each $\sim 40\mu m$ long for a total trap length of $\sim 120\mu m$. In addition to this, the atoms are also subject to a magnetic field tuned to the Feshbach resonance making them strongly interacting and allowing the ones in the middle to become a superfluid. This trap is preferred compared to others since it provides a nice apparatus for conducting novel equilibrium experiments as well as a uniform potential profile that simplifies our system.

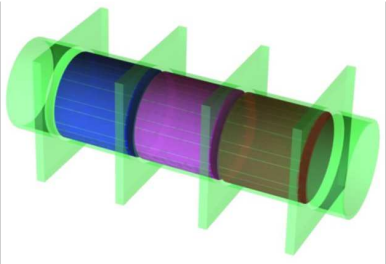

Figure 1: The multi-region trap separated into three regions: isolated spin up/down polarized atoms on either end with a superfluid mix in the middle.

3.2 Joule Expansion

One of the first experiments we can perform on the atoms before having the entire multi-region trap set up is a Joule expansion experiment where we isolate all atoms to one side of the trap with a light sheet and then remove the barrier to study their dynamics as they move into the vacuum. Technically, this can be performed after evaporative cooling occurs in the ODT because it only requires one light sheet at the center of the trap separating the atoms from the vacuum and removing the light sheet to allow for expansion. However, since the ODT uses a harmonic potential the matter is not evenly distributed in its side of the trap as its density is a function of radial distance. This means that we would have to be cautious to account for the non-uniform distribution when modeling the system. This is precisely why the multi-region trap will use a box trap potential profile, which is essentially where the profile is uniform everywhere within the trap. This then makes the Joule expansion and other types of experiments easier to model and understand.

3.3 Transport in Multi-Region Trap

With the multi-region trap fully in tact and loaded with atoms, we would also be able to study the spin transport and evolution of the spin current that is present when the three regions are joined together again, known as the *transport through the bulk* experiment. As shown in Fig.2, the regions can effectively be joined together again by continuously ramping down both of the middle light sheets until the trapping potential of the sheet is low enough that atoms can start tunneling through. The different chemical potentials of the spin species will drive the spin transport causing the left reservoir to diffuse to the right and the right reservoir to diffuse to the left. By taking pictures to measure the atom flux through the z=0 plane, we can find calculate the spin current J_s present in the system. If we also take pictures of each outer region to measure the densities of the spin up $n_\uparrow$ and spin down $n_\downarrow$ species, then we can use a formula for spin current

$$\vec{\mathbf{J}}_s = -D_s \vec{\nabla}(n_\uparrow - n_\downarrow) \tag{3}$$

to find the spin transport coefficient D_s which characterizes the evolution of the spin current.

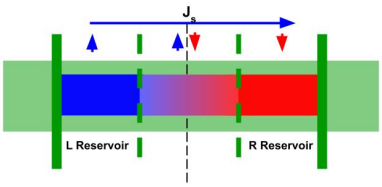

Figure 2: Demonstration of the transport through the bulk experiment with the two inner light sheets being ramped down and our z=0 plane defined as the dotted line in the middle

We will also use the multi-region trap to examine *transport through normal-superfluid interfaces*. As shown in Fig.3, this experiment is very similar to the transport through the bulk with the primary difference being that we only ramp down one of the inside light sheets and observe how the system comes to equilibrium. Although we have a theoretical basis for what to expect at this interface [7], this would be a novel experiment to perform and see how well the experiment matches the theory. As opposed to the transport through the bulk, this experiment will be focused on finding the rate of atoms flowing across the interface as a function of the polarizations in the two regions.

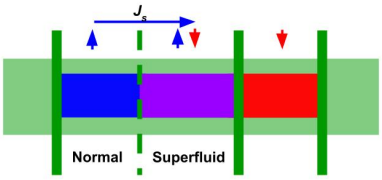

Figure 3: Demonstration of the normal-superfluid interface experiment where only one of the inner light sheets is ramped down to induce transport. In contrast to the through the bulk experiment, we define the z=0 plane here to be at the same location as the light sheet being ramped down.

4 Light Sheet Implementation

4.1 DMD

To help shape the intensity profiles of the light sheets in an efficient way, we utilize a digital micro-mirror device (DMD) which is a rectangular array of over four million microscopic mirrors that can be individually controlled to be rotated into an $\pm 12°$ on/off position as shown in Figure 4a. Because the DMD is made up of individual mirrors that have tiny gaps between each other, it behaves like a diffraction grating. This means that when the laser light is shined onto the DMD, it will be split up into the different diffraction orders of light each of which will be reflected off the DMD at a different angle. As a result, in order to get the most amount of power out of the beam from the reflection, we must orient the DMD at the right angle of incidence to optimize the imaging system for the zeroth-order beam (the most intense order) which is 24° away from normal incidence. In a similar fashion, the DMD must also be oriented at the right vertical angle in order to ensure the beam is only reflected horizontally. Although we know the tilt of the mirrors, since the tilt is along the diagonal, per Figure 4b, we know that the vertical tilt will be a factor of $\sqrt{2}$ smaller than the total tilt, meaning that the DMD must be tilted $\sim 8°$ towards the horizontal so that when mirrors are in the ON state they are vertically normal to the beam.

In addition to shaping the intensity profile, which will be discussed in detail in the following sections, the DMD can also act as a switch for the light sheets produced in the experiment. With its 10 kHz refresh rate, the DMD makes a handy tool that can be used to control the exposure of the light sheets to the atoms. This is due to the fact that the entire experiment, from the beginning stage of cooling to imaging the atoms in the box trap, takes place over the span of over a few seconds. As a result, the light sheets from the DMD will only need to be shined on the atoms for a fraction of a second near the end of the experiment.

Along with that, the preciseness of the refresh rate is essential for conducting our experiments in a controlled manner. If we cut off the entire light sheet abruptly, then the atoms in each region would collide with each other relatively violently introducing complexities in their evolution that make it harder to characterize the system. With a fast enough refresh rate, however, the DMD can be programmed with a sequence of patterns that ramp down the intensity of the light in an effectively continuous way. This softens the collisions the atoms feel and allows us to measure the spin transport coefficient more accurately.

4.2 Imaging System

Once the beam(s) are properly prepared and aligned, the plane of the DMD is imaged using a series of lenses and mirrors that effectively magnify the system by a factor of 0.1. This is partly due to the fact that the light sheets produced by the DMD are much too large to be used effectively

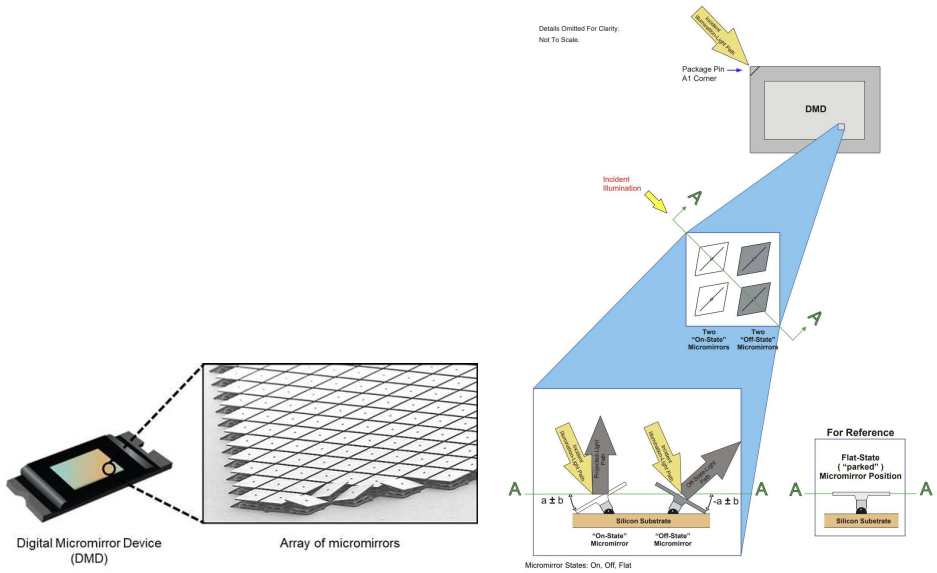

(a) (b)

Figure 4: (a) A close up view of the array of mirrors for the DMD[5]. (b) Shows the three possible orientations for each mirror. Rather than being tilted strictly horizontally/vertically, each mirror can instead be rotated $\approx 12°$ in each direction about its main diagonal, or about an axis 45° above the horizontal.[3]

in the multi-region trap; we want the light sheets to be about $3-4\mu m$ thick so they can fit with our dimensions described in Sect.3.1. In addition to this, the magnification of the imaging system is essential for the process of halftoning (see Sect.4.3.2) because of the point spread function (PSF) for the beam. The point spread function describes how the rays of an object propagate through the optical system allowing us to compare the image plane to the object plane. After reflecting the light, each DMD mirror can be modeled as a point source with their own PSF and it becomes apparent that demagnifying the light sheets will cause overlap of the PSF of adjacent mirrors. This overlap onto the pixels of produces the desired flat top intensity profile for the light sheets when combined with halftoning. On top of this, after being reflected off of the DMD, the light, as can be seen in Fig.5, passes through an imaging system consisting of a $1000mm$ lens followed by a $100mm$ lens. From linear optics, we know that these lenses will produce a magnification of $M = -\frac{f_3}{f_2} = -0.1$. By shrinking the DMD image down, we cause the PSF's of each ray to increase their overlap and making halftoning work better. Although this will successfully image the DMD plane onto the camera, an analysis of the camera data is necessary to finding characteristic values of the light sheet such as its resolution. In particular, the light sheet's PSF (roughly a Gaussian) is convolved with a step function (representing the mirrors ON/OFF cutoff) to output a semi-Gaussian function. One horizontal slice is taken from the image capturing the peaks and the data is fit to the convolved function to find the width parameter for each.

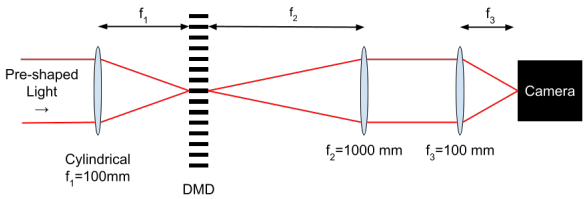

Figure 5: The light sheets are demagnified by a factor of 10 as they pass through the imaging system before they hit the camera.

4.3 No Pre-shaping

4.3.1 Direct Illumination Light Sheets

The simplest way to achieve light sheets from our set up is to shine a Gaussian beam onto the DMD and program it to only turn on mirrors in an array of four rectangles regularly spaced apart. Since we are choosing what light to keep from the beam, the thickness, and thus resolution, of the light sheets can be set directly as demonstrated in Fig.. Using this setup, we are able to achieve light sheets with thickness $2.6\mu m$. With a diffraction limit of $2.3\mu m$ for our system, this suggests that there is some aberration present, but this is still a very good imaging system. We also measure the trapping potential of the light sheets as a function of laser power output to see how much light we are losing with the DMD. As can be seen in Fig.7, the direct illumination or "regular" light sheets have a trapping potential comparable to the trapping potential of the entire beam itself. While this does produce light sheets in a strict sense, because the beam is roughly Gaussian (see the left image in Fig.8a) to start the intensity profile of the reflected light sheets will also be Gaussian.

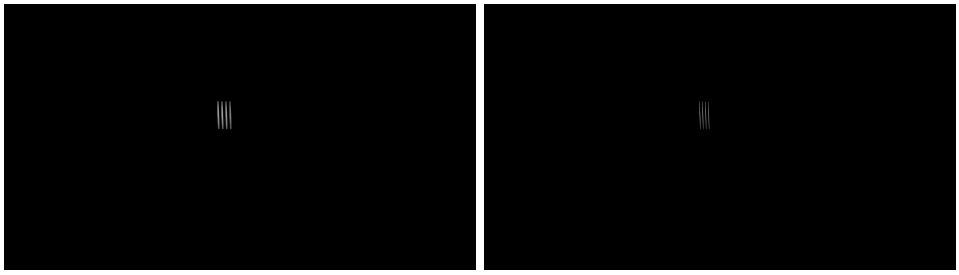

(a) Direct illumination light sheets using a width of 40 pixels

(b) Direct illumination sheets using a width of 15 pixels

This is a problem, though, because performing the experiments discussed in Sect.3 requires ramping down the light sheets separating the relevant regions in a continuous, gradual fashion so as to keep the dynamics of the system as simple as possible. However, if the intensity profile is roughly Gaussian then that means that the probability of atoms tunneling through the light sheet into the different region is greater on the edges of the light sheet than in the center creating a non-uniform atom flux. This probability distribution will make the system more complex and harder to accurately measure the values we're looking for. So, we need a way to flatten this profile which is where halftoning enters the picture.

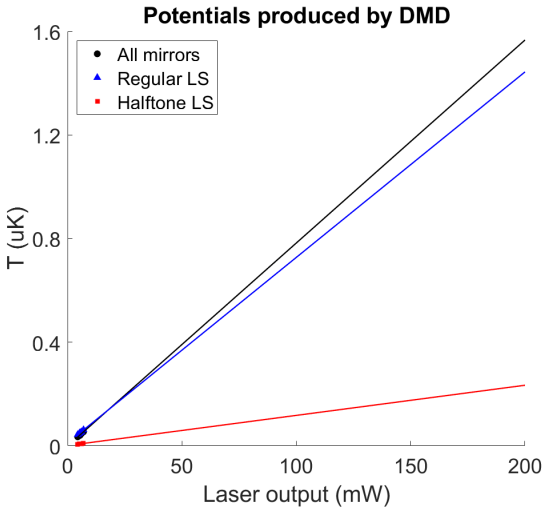

Figure 7: Graph showcasing the trap potential energy as a function of laser power input. By using the relation $U = k_B T$, where k_B is the Boltzmann constant, we can easily quantify the depth of the potential well using temperature.

4.3.2 Halftoned Light Sheets

Drawing its roots from print halftoning where the white space of the paper is exploited in tandem with the size and distribution of colored dots to create a smooth, gradient effect in color, *digital halftoning*, otherwise known as grayscale rendering or spatial dithering, is the practice of instead exploiting the black environment of the camera by turning off certain pixels to again create this smooth effect on a screen[6]. Applying this to our case, we can utilize an error diffusion algorithm (EDA) to turn off certain mirrors on the DMD to create a smoothing effect on the intensity profile of the light as shown in Figure 8a.

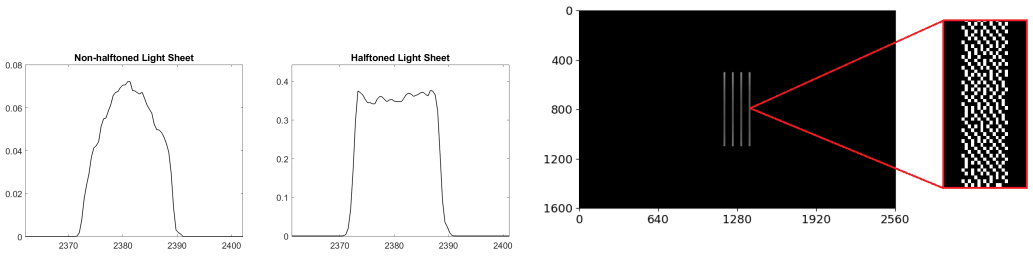

(a) (b)

Figure 8: (a) These are graphs of intensity vs. horizontal pixel location on the DMD. We see the how the normal light sheets produce a Gaussian intensity (left) while the error diffusion algorithm determines a halftoning pattern that gives an almost uniform intensity across the sheet (right) (b) Example of a half-toned pattern that results in the flat-top intensity profile

The EDA works by effectively averaging out errors associated with each pixel to its neighbors so as to smooth out the intensity and output the desirable profile. The EDA is fundamentally based on trying to map a target function $t(m, n)$ describing intensity on an mxn grid of pixels (which can take any value within the range [0,1]) onto a binarized function $s(m, n)$ (meaning it can only take on values of 0 or 1) representing the on/off pixels on the DMD. As we can see from the flow chart in Fig.9, by finding the error $e(m, n)$ between $t(m, n)$ and the associated binary output $s(m, n)$ we can adjust the target values of the nearest neighbors by an amount based on $e(m, n)$ and a weighting parameter $c(a, b)$. This is done lexicographically for all relevant pixels on the DMD at which point $s(m, n)$ is returned which we can program onto the DMD for a smooth intensity profile.

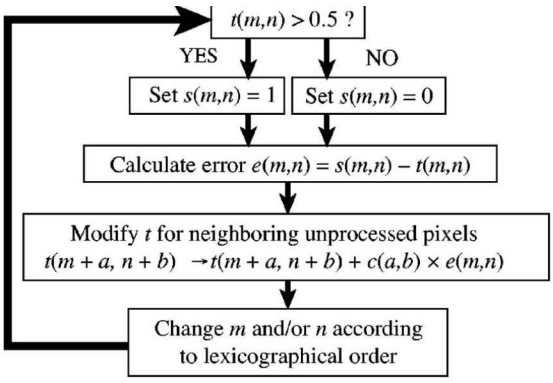

Figure 9: From Ref.[2]

While this pattern works to create uniform intensity light sheets, we quickly run into the problem of low efficiency in power output. This makes sense because in order to achieve halftoning, it is a necessity to take away some input light, meaning that the intensity can only go down as a result. As we can see in Figure 7, the regular light sheet intensity pattern is almost as efficient as simply having all the mirrors on while the halftoned light sheets have significantly lower trapping potentials. According to the graph, the lithium atoms would have to have a temperature on the order of $100nK$ or lower in

order for the half-toned light to hold it which would require much more cooling of the atoms. Not only would this require a more extensive cooling process to prepare the atoms, but it would also effectively bar us from performing any higher temperature experiments since all the atoms would escape as soon as they were warm enough. Luckily, there is a way to mitigate this by first pre-shaping the beams into light sheets before they hit the DMD.

4.4 Preshaping

4.4.1 Optical Set Up

In order to improve the efficiency of the light, we want to maintain the shape of the light but without the excess waste of power from all the light not hitting a mirrored region on the DMD. To mitigate this loss, we simply choose to shape the beams into their light sheet form before they are incident upon the DMD. To do this, we utilize a simple optical set up in which we make four beams by splitting an initial laser beam three times with beam-splitter cubes. Notably, we make use of D-shaped mirrors, which are essentially just mirrors split down the middle shown in Fig.10a, to bring the beams as close together as possible. Once the four beams are realized, they then pass through a cylindrical lens which focuses the light along one direction (perpendicular to the cylindrical axis of the lens indicated by the orange arrow in Fig.10b) and forms the desired light sheets. With this pre-shaped light we can ensure that as much light as possible is hitting the rectangular array of mirrors (by either adjusting the beam location or the programmed mirror patterns), boosting its intensity and efficiency.

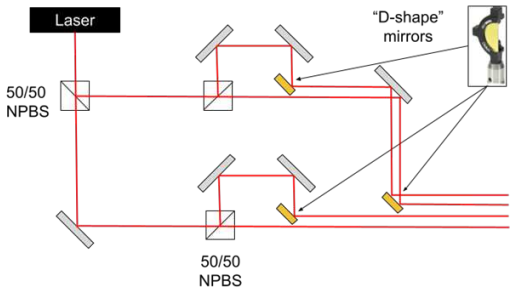

(a) Top-down diagram of the preshaping optical setup

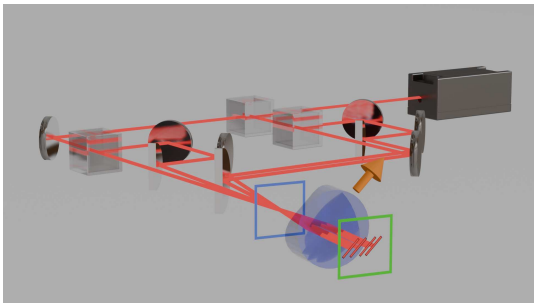

(b) 3D view of the same set up to show the intersection of all beams in the Fourier plane (blue outline) as well as the effect of the cylindrical lens on each beam

4.4.2 Ray Matrix Analysis

For any optical set up, it is possible for one to derive ray transfer matrices that can describe the evolution of the light rays as they pass through each element. We will take advantage of this to develop a model of our optical system from the D-shaped mirrors to the focal plane on the DMD so that we can identify optimal parameters for our beams. We start by identifying the coordinate system of our D-shaped mirror, shown in Fig.11 , and then we can begin solving for the ray matrices. If the optical axis is an axis of symmetry, then our model only needs to take into account one of the perpendicular directions. However, if the system contains astigmatic elements, such as a cylindrical lens, then we must keep track of both transverse components since they will be affected differently.

In our case, the system can be regarded as having simple astigmatism and can therefore be analyzed using a 2x2 matrix for each direction taken into account, or a 4x4 matrix in total. In addition to the ray's position, its angle of propagation for each direction is necessary for obtaining an accurate model of the system. Generally, we can find that the rays transform according to the matrix equation

$$\begin{pmatrix} x \\ x' \\ y \\ y' \end{pmatrix} = \begin{pmatrix} A_x & B_x & 0 & 0 \\ C_x & B_x & 0 & 0 \\ 0 & 0 & A_y & B_y \\ 0 & 0 & C_y & D_y \end{pmatrix} \begin{pmatrix} a \\ a' \\ b \\ b' \end{pmatrix} \tag{4}$$

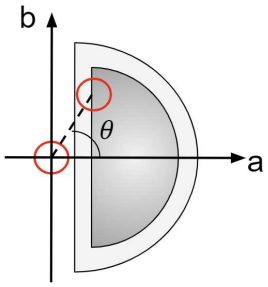

Figure 11: Our coordinate system origin is defined to coincide with the beam that passes by the D-shaped mirror. Here, two beams are located at the centers of the red circles and we see that alignment conditions were met so the resulting light sheets are aligned.

where *x, y* and *x', y'* are the positions and angles, respectively, with respect to the optical axis in the *output* plane whereas *a, b* and *a', b'* measure the same qualities in the *input* plane. In order to fully describe our optical system, the total ray matrix in equation 4, which we'll denote as M_{tot}, must include information about the cylindrical axis and its ability to rotate the focusing axis M_{cyl} as well as the free space propagation $M_{\text{fsp}}(z)$ before and after the cylindrical lens. If the beam travels a distance d from the DMD to the lens and then travels the focal distance f after the lens to be imaged, then we can construct the matrix equation for the entire system (read right to left) to be

$$\mathbf{M}_{tot} = \mathbf{M}_{fsp}(f)\mathbf{M}_{cyl}\mathbf{M}_{fsp}(d). \tag{5}$$

Now, our only challenge is findind the right matrices to describe each optical element. We can start by simplifying equation 4 by grouping together related elements in the matrices like so:

$$\begin{pmatrix}\mathbf{x}\\ \mathbf{y}\end{pmatrix} = \begin{pmatrix}\mathbf{M}_x & \\ & \mathbf{M}_y\end{pmatrix}\begin{pmatrix}\mathbf{a}\\ \mathbf{b}\end{pmatrix}. \tag{6}$$

Here, $\mathbf{M}_x$ and $\mathbf{M}_y$ are matrices describing the effect of the cylindrical lens with focal length f assuming that it focuses along the x-axis and neglecting the effect of rotation. They are given by

$$\mathbf{M}_x = \begin{pmatrix}1 & 0\\ -\frac{1}{f} & 1\end{pmatrix};\ \mathbf{M}_y = \begin{pmatrix}1 & 0\\ 0 & 1\end{pmatrix}. \tag{7}$$

Taking into account our ability to rotate the cylindrical lens about the optical axis will modify the total matrix for the lens into

$$\mathbf{M}_{cyl} = \begin{pmatrix} 1 & 0 & 0 & 0\\ -\frac{\cos^2\theta}{f} & 1 & -\frac{\sin\theta\cos\theta}{f} & 0\\ 0 & 0 & 1 & 0\\ -\frac{\sin\theta\cos\theta}{f} & 0 & -\frac{\sin^2\theta}{f} & 0\end{pmatrix}. \tag{8}$$

Finally, we can describe the free space propagation for both transverse directions of the beam with the matrix

$$\mathbf{M}_{fsp}(z) = \begin{pmatrix}1 & z & 0 & 0\\ 0 & 1 & 0 & 0\\ 0 & 0 & 1 & z\\ 0 & 0 & 0 & 1\end{pmatrix} \tag{9}$$

which is the last piece of the puzzle to describing this system. Now, we can find relations between the input and output plane coordinates so that we can have a mathematical basis for optimizing our setup. Plugging in equation 5 to equation 6 gives us the following system of equations

$$x = a'f + \gamma\sin\theta \tag{10}$$

$$y = b'f - \gamma\cos\theta \tag{11}$$

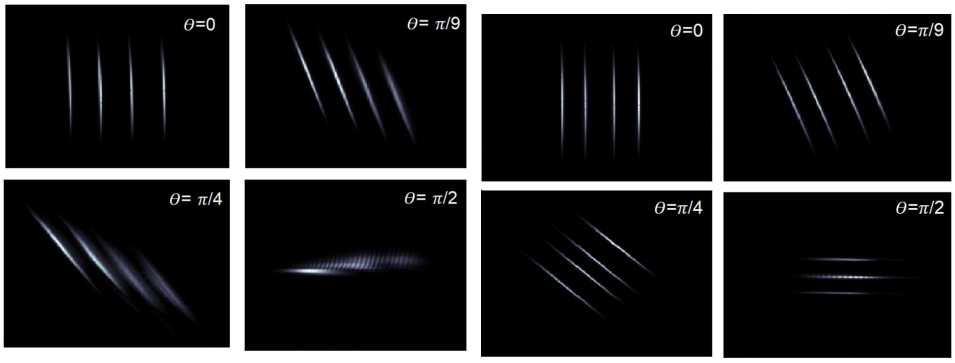

(a) (b)

Figure 12: (a) A series of light sheets with different θ values for the cylindrical lens without adhering to alignment conditions (b) Rotations of the cylindrical lens while maintaining alignment conditions. Note that the D-shape orientation for these pictures is the same as in Fig.11, hence we are unable to align the light sheets at $\theta = \frac{\pi}{2}$ while maintaining the condition $x' = y' = 0$

$$x' = a' - \frac{\sigma \cos\theta}{f} \tag{12}$$

$$y' = b' - \frac{\sigma \sin\theta}{f} \tag{13}$$

where

$$\gamma = (a + a'd)\sin\theta - (b + b'd)\cos\theta \tag{14}$$

$$\sigma = (a + a'd)\cos\theta + (b + b'd)\sin\theta \tag{15}$$

With a full description in hand, we can now begin to place restrictions on the system to match our desired set up. The first restriction we will place is the *alignment condition* which requires that all of the light sheets have their centers lie on a normal line to all of the light sheets. This can be modeled by

$$b'\cos\theta - a'\sin\theta = \frac{a\sin\theta - b\cos\theta}{f + d} \tag{16}$$

which ensures that any pair of light sheets whose positions and angles satisfy the equation will be aligned. Going further, when the light sheets are imaged onto the trap we would ideally want the normal vectors of both the ring beam and the light sheets to be parallel, the *idealized alignment condition*. In other words, we want the sheets to intersect the ring beam with as little relative angle as possible. This imposes yet another restriction in the form of setting $x' = y' = 0$ which, when plugged into equations 10-13, gives us the clean and concise restriction

$$\frac{b}{a} = \frac{b'}{a'} = \tan\theta. \tag{17}$$

By analyzing equation 17, we can readily identify geometrical constraints on the possible alignments depending on the angle θ. For example, taking the $\theta = 0$ case we immediately see that in order for the light sheets to satisfy the idealized alignment condition it requires $b = b' = 0$. Assuming the same mirror orientation as shown in Fig.11, this doesn't present a problem. If, however, we were to rotate the cylindrical lens to have $\theta = \frac{\pi}{2}$, the idealized alignment condition would require $a = a' = 0$ instead which is impossible to achieve without first rotating the mirror, as can be seen in Fig. 12b.

4.4.3 Normal Light Sheets

With the preshaping set up intact, light sheets can be produced in ways similar to the methods described in Sect.4.3.1 and 4.3.2. From there, the DMD can be programmed to reflect the preshaped beams by turning on all the mirrors within a range that encompasses all of the light to give more

intensity to the light sheets. However, this comes at a cost to the sharpness of the sheets. By instead programming the DMD to only turn on small, rectangular regions of mirrors centered on each preshaped beam, the sharp cutoff of the regions maintains the desired high resolution of the sheets. Although we would like our light sheets to have high resolution i.e. small beam widths to obtain maximum trapping potential, we also don't want the ligth sheets to be too thin either. This is because the smaller the minimum waist w_0 of a beam is, the faster it will diverge after the focal plane of the image plane. So, making the sheets too thin would cause the intensity to fluctuate within the box trap, creating a non-uniform tunneling probability for the atoms which will make it harder to accurately measure system quantities. To mitigate this, we need to find the smallest w_0 that would allow the beam of the light sheet to be considered roughly collimated within the region of the trap. We can calculate this value to be $\approx 2\mu m$, which means that any sheet with a $w_0 \geq 2\mu m$ can be considered roughly collimated inside the trap. So, although not as sharp as the direct illumination case, we were able to achieve light sheet thicknesses between $3.5 - 4.5\mu m$ which is satisfies our requirements for what we want to accomplish In addition to that, we were able to obtain even better trapping potentials than the non-preshaped direct illumination case. For one light sheet produced (i.e. the laser is not split into separate beams but instead is directly preshaped by the cylindrical lens and imaged on the DMD) we were able to get a trapping temperature of $40\mu K$ while the four light sheet set up yielded a peak trapping temperature of $10\mu K$, which is what we would expect after using two 50/50 beam splitter cubes in our optical set up.

4.4.4 Halftoned Light Sheets

As shown in Sect.4.4.3, by preshaping the beams incident on the DMD, we can significantly improve the maximum output intensity to give us stronger light sheets with sufficient resolution. The intensity can then be flattened by utilizing the techniques of halftoning described in Sect.4.3.2. In the same way as the non-preshaped case, the error diffusion algorithm will systematically decide which mirrors to turn off in order to output the flat potential profile required for the light sheets. At the moment, however, we are unable to realize effective halftoning with the preshaped light sheets like we were for the non-preshaped sheets. One potential reason for this is that the relative angle between the DMD and the light sheets (from the tilt or relative angle of the mount discussed in Sect.4.1, small fluctuations/misalignment of x' or y', etc.) can make it challenging to ensure all four beams are safely within the focal plane of the cylindrical lens. If the focal plane is not close enough to the surface of the DMD, then the light sheets won't be as focused as they could be. This will increase their width and therefore alter the $t(m, n)$ function we measure which can drastically change the outcome of the EDA.

5 Outlook

With sufficient trapping potentials and light sheet resolutions reached, one obstacle ahead of us at the moment is troubleshooting the halftoning error with the preshaped light sheets. Once we can correct this error and obtain a flat intensity profile for the light sheets, we can move on to implementing this optical set up onto the main experiment table. From there, the optical set up will be primed to shine its light sheets onto the ring beam and create our multi-region box trap. After that, the only thing to do would be to perform our Joule expansion, transport through the bulk, and transport through the normal-superfluid interface and work to characterize the behavior of the spin current.

References

[1] Christopher Kenneth Angyal. "Optical trapping of 6LI for studies of transport in strongly interacting fermions". PhD thesis. ProQuest Dissertations Theses, 2023.

[2] Christophe Dorrer and Jonathan D. Zuegel. "Design and analysis of binary beam shapers using error diffusion". In: *J. Opt. Soc. Am. B* 24.6 (2007), pp. 1268–1275. DOI: 10.1364/JOSAB.24.001268. URL: https://opg.optica.org/josab/abstract.cfm?URI=josab-24-6-1268.

[3] *Family of 0.9 WQXGA Type A DMDs*. DLP9000. Rev. B. Texas Instruments. 2016. URL: https://www.ti.com/lit/ds/symlink/dlp9000.pdf?ts=1715960108586&ref_url=https%253A%252F%252Fwww.ti.com%252Fproduct%252FDLP9000%253Fqgpn%253Ddlp9000.

[4] Rudolf Grimm, Matthias Weidemuller, and Yu. B. Ovchinnikov. "Optical dipole traps for neutral atoms". In: *Advances in Atomic Molecular and Optical Physics* 42 (1999), pp. 95–170. URL: https://api.semanticscholar.org/CorpusID:16499267.

[5] Pernille Kennedy. *How does a DMD spectrometer work? - recorded webinar*. 2021. URL: https://ibsen.com/how-does-a-dmd-spectrometer-work/.

[6] Robert Ulichney. *Digital halftoning*. MIT Press, 1996.

[7] Ding Zhang and Ariel T. Sommer. "Transport of spin and mass at normal-superfluid interfaces in the unitary Fermi gas". In: *Physical Review Research* 4.2 (June 2022). ISSN: 2643-1564. DOI: 10.1103/physrevresearch.4.023231. URL: http://dx.doi.org/10.1103/PhysRevResearch.4.023231.